Cellulose (2013) 20:2991–3005
DOI 10.1007/s10570-013-0061-x

ORIGINAL PAPER

Crosslinked nanofibrillated cellulose: poly(acrylic acid) nanocomposite films; enhanced mechanical performance in aqueous environments

Steven Spoljaric · Arto Salminen · Nguyen Dang Luong · Jukka Seppälä

Received: 12 June 2013 / Accepted: 17 September 2013 / Published online: 25 September 2013

Abstract Nanofibrillated cellulose (NFC) was compounded with poly(acrylic acid) (PAA) via solvent casting. Nanocomposite films were thermally-crosslinked to allow the formation of ester bonds between NFC and PAA, as confirmed by ^{13}CNMR and infrared spectroscopy. The network morphology of the cellulose nanofibrils was left intact by the introduction of PAA and crosslinking. Water absorption and swelling was diminished by the introduction of crosslinking, due to the reduced number of vacant hydroxyl and carboxyl groups available to interact with water molecules. Crosslinking with PAA increased the activation energy required for thermal degradation. PAA effectively reinforced NFC, increasing Young's modulus, tensile strength and glass transition temperature. Crosslinking imparted restraints on segmental motion of polymer chains, further enhancing the thermomechanical properties and retaining elasticity. Wet-strength properties were enhanced due to the reduced hydrophilicity of crosslinked nanocomposite films.

S. Spoljaric · A. Salminen · N. D. Luong · J. Seppälä (✉)
Polymer Technology, Department of Biotechnology and Chemical Technology, Aalto University School of Chemical Technology, P.O. Box 16100, 00076 Aalto, Finland
e-mail: jukka.seppala@aalto.fi

Keywords Nanofibrillated cellulose · Poly(acrylic acid) · Crosslinking · Nanocomposites · Mechanical testing

Introduction

Nanocellulose derivatives are rapidly becoming a promising and important material, fueled by the shift in research trends towards 'greener' and environmentally friendly materials. Of the various nanocellulose materials, nanofibrillated cellulose (NFC) has attracted much interest due to its remarkable stiffness, mechanical and barrier properties and ability to form networks at low concentrations. These characteristics are derived from NFC's high aspect ratio (4–20 nm wide, 500–2,000 nm in length), allowing the nanofibrils to form strong interactions amongst themselves and with surrounding molecules/polymers (Klemm et al. 2011). NFC has readily been incorporated as reinforcement into polymer matrices (Al-Turaif 2013; Endo et al. 2013; Fujisawa et al. 2012; Littunen et al. 2013), with nanocomposites exhibiting enhanced tensile mechanical properties (Nakagaito and Yano 2005) compared to conventional wood-pulp reinforced composites. The fibril's nano-scale diameter is below the wavelength of visible light, allowing NFC to be compounded with polymer matrices without altering optical properties (Nogi et al. 2005). In

addition, NFC is non-toxic, biodegradable and renewable (Fox et al. 2012).

Several challenges and limitations are present in the utilisation of NFC. Lignocellulosic fibres' polar structure (facilitated by the vast number of hydroxyl groups) and subsequent hydrophilic nature results in incompatibility between NFC and many polyolefins and thermoplastics, unless chemical or physical treatment of the nanofibrils is performed. Compounding NFC with a hydrophobic matrix generally results in filler agglomeration and inadequate matrix-fibre interaction. This weak interface can potentially deteriorate composite mechanical, thermal and other properties. Furthermore, cellulose fibrils readily absorb moisture due to their polar structure, leading to reduced material stability, mechanical and water barrier properties. Processing conditions and polymer choice are limited since cellulose fibres begin to thermally degrade at ~200 °C (Moon et al. 2011). And finally, NFC possesses inherently poor elastic and tear-strength behaviour.

Various polar and water-soluble polymers have been compounded with NFC in an effort to retain or enhance material properties. Amongst the most common, poly(vinyl alcohol) (PVA) is one of the most widely studied (Cho and Park 2011; Lee et al. 2009; Paralikar et al. 2008; Peresin et al. 2010; Srithep et al. 2012), with nanocomposites yielding enhanced mechanical and barrier properties. To overcome PVA's poor moisture stability (Priest 1951), poly(-acrylic acid) (PAA) has been utilised as a crosslinking agent (Baştürk et al. 2013; Kim et al. 2005; Kumeta et al. 2003; Li and Hsieh 2005; Paralikar et al. 2008). The thermally-activated crosslinking reaction results in ester formation between the hydroxyl groups and carboxylic acid. The method is simple, effective, fast and occurs without the formation of toxic side products. Due to the numerous hydroxyl group present within NFC, it is highly likely that PAA can interact with and crosslink the nanofibrils in addition to PVA. Clemons et al. (2013) obtained similar conclusions regarding this multi-component interaction using chemical imaging. However, they found that PAA was prone to migrating out of the PVA into surrounding NFC regions, weakening the interface and reducing stress-transfer efficiency.

Directly crosslinking the NFC network may prevent the formation of a weakened interface and enhance intrinsic mechanical and barrier properties. Syverud et al. (2011) prepared cryo-structured gels by crosslinking nanocellulose fibrils with poly(ethyleneimine) and poly(N-isopropylacrylamide-co-allylamine-co-methylenebisacrylamide). The prepared gels exhibited enhanced elasticity and regained their original shape following the release of applied pressure. Electrospun cellulose nanocrystal-PAA fibrous membranes prepared by Lu and Hsieh (2009) displayed enhanced tensile mechanical properties and reduced hydrophilicity. Crosslinking the membranes doubled the Young's modulus and quadrupled maximum stress. Although PAA has been compounded with various nanocellulose forms and derivatives (Dubolazov et al. 2006; Loría-Bastarrachea et al. 2002; Luo et al. 2013; Nikolaeva et al. 2000; Şakar-Deliormanli 2012) to the best of the authors' knowledge no studies have been performed regarding NFC-PAA nanocomposites or the crosslinking of NFC with PAA. Furthermore, the majority of compounding techniques involve grafting, polymerisation or other advanced processing/fabrication methods. This provides an opportunity to examine solution casting (and subsequent thermally-induced crosslinking) as an effective and simple method of preparing crosslinked NFC-PAA nanocomposite films with enhanced intrinsic properties.

The aim of this research was to determine the influence of PAA concentration and crosslinking on the material properties of NFC. Crosslinking has been successfully utilised to enhance NFC properties, including mechanical, thermal and barrier. Furthermore, there is great environmental and economic benefit in preparing nanocomposites with the highest possible NFC concentration, highlighting the importance of optimising the NFC-PAA ratio within the nanocomposite films. Solvent casting was utilised to prepare nanocomposite films, while the mechanical, thermal, morphological and solubility properties were characterised.

Experimental

Materials

Nanofibrillated cellulose (NFC) was provided by UPM Corporation (Helsinki, Finland), under the product name UPM Fibril Cellulose. The NFC was prepared via mechanical disintegration of bleached

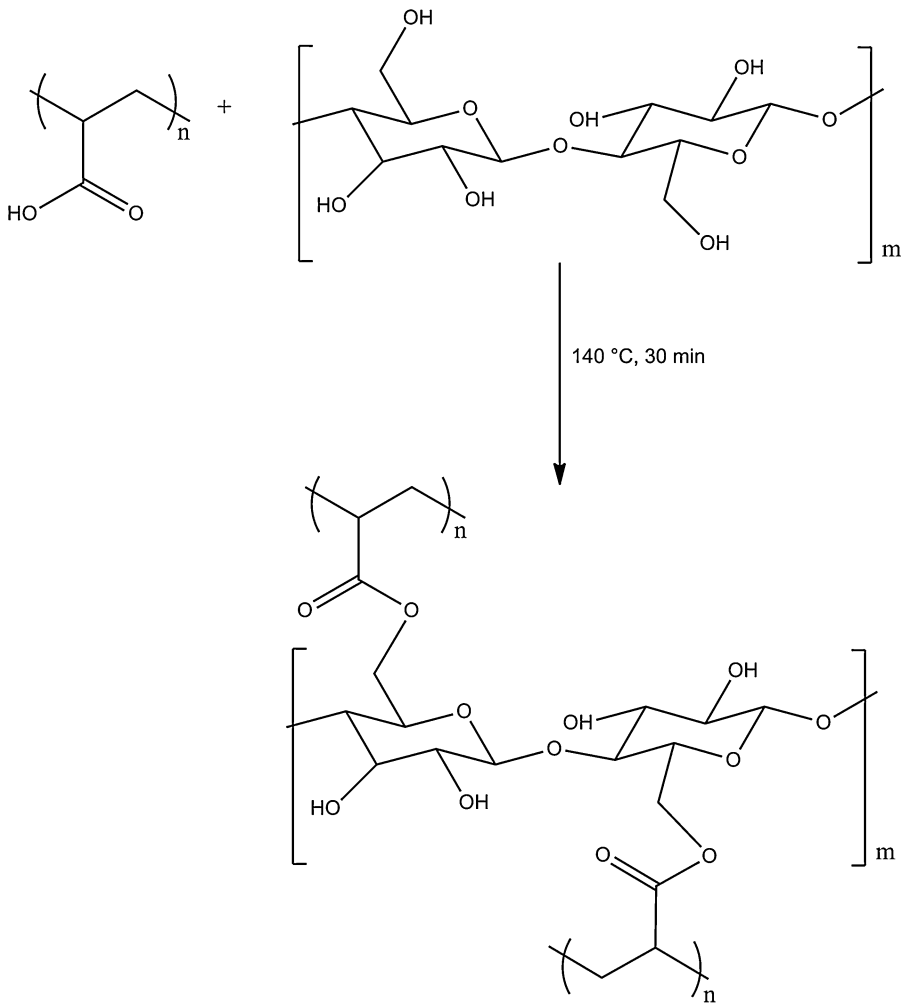

Scheme 1 Esterification reaction between PAA and NFC

birch pulp, which was pre-treated with a Voith refiner. The material was subsequently fluidised by seven passes through a M7115 fluidiser (Microfluidics Corp, Newton MA, USA). The solids content of the prepared dispersion was 1.39 wt%. Poly(acrylic acid) (PAA, $M_w = 450{,}000$) was provided by Sigma Aldrich, USA.

Preparation of nanocomposites

Nanocomposites were prepared via a solution casting method. Appropriate amounts of NFC and 5 wt% PAA solution were mechanically stirred at room temperature for 2 h (700 rpm). Prior to stirring, additional Milli-Q water was introduced to adjust the total solid content to 1.1 wt%. The nanocomposite solutions were degassed for 20 min using a Branson 5510 sonicator, then cast into polystyrene petri dishes. The films were allowed to dry in air at 23 °C and 50 % relative humidity before being dried in an oven (non-crosslinked films: 120 °C, 20 min). Crosslinking was performed by placing the films in an oven at 140 °C for 30 min. The (esterification) crosslinking reaction between PAA and NFC is presented in Scheme 1. Films were kept in a vacuum oven for 24 h at 60 °C before being stored at 23 °C and 50 % relative humidity. Films were kept under these conditions for at least 7 days prior to testing, in order for the films to stabilise. PAA was added in concentrations of 5, 10, 25 and 50 wt%.

Characterisation of nanocomposites

Solid-state ^{13}C NMR

Solid state ^{13}C cross polarisation magic angle spinning (CP MAS) NMR spectra of NFC-PAA nanocomposites were recorded with a Bruker AVANCE-III 400 MHz spectrometer operating at 100.6 MHz for ^{13}C. The spinning speed of samples was 8000 Hz, contact time 2 ms and delay between pulses 5 s.

Attenuated total reflectance infrared spectroscopy (ATR-FTIR)

A Unicam Mattson 3000 FTIR spectrometer equipped with PIKE Technologies GladiATR (with diamond crystal plate) was used to characterise the chemical structure of the nanocomposites. All spectra were scanned within the range 400–4000 cm^{-1}, with a total of 16 scans and a resolution of 32 cm^{-1}.

Scanning electron microscopy (SEM)

A Zeiss SIGMA VP scanning electron microscope operating at 3 kV was used to characterise the morphology of the nanocomposites. Composites with average dimensions $\sim 5.00 \times 5.00 \times 0.05$ mm^3 were mounted to the specimen holder using carbon tape.

Crosslink density

The crosslink density of the nanocomposites was determined using a swelling method and Flory-Rhener theory as displayed in Eq. 1;

$$\rho_e = \frac{\left[\ln\left(1-\upsilon_{2,s}\right)+\upsilon_{2,s}+\chi_1\left(\upsilon_{2,s}\right)^2\right]/V_1}{\left(\upsilon_{2,s}^{1/3}-\frac{\upsilon_{2,s}}{2}\right)} \quad (1)$$

where $\chi_1$is the Flory–Huggins polymer–solvent dimensionless interaction term for cellulose-water (0.44), V_1 is the molar volume of solvent and $\upsilon_{2,s}$ is the polymer fraction volume.

Water absorption and swelling

Films were weighed and submerged in Milli-Q water at 23 °C. Specimens were periodically removed, wiped with a tissue to remove excess water and weighed. The submerged films were stored at 50 % relative humidity and all specimens were characterised in duplicate. The swelling degree was calculated using Eq. 2;

$$\text{Swelling degree} = (W_s - W_d) \,/\, W_d \cdot 100\% \quad (2)$$

where W_s is the weight of the film in the swollen state and W_d is the weight of the film in the dry state.

Thermogravimetric analysis (TGA)

A TA Instruments Q8000 thermogravimetric analyser was used to characterise the thermal stability and degradation behaviour of the nanocomposites. Samples of $\sim$10 mg were heated to 850 °C at 20 °C min^{-1} in an inert environment provided by a 20 mL min^{-1} nitrogen purge.

Stress–strain analysis

Stress–strain analysis was performed using an Instron Universal Testing Instrument, Model 33R4204 with a 100 N static load attached. A strain rate of 0.5 mm min^{-1} was applied to each sample (average dimensions: $20.00 \times 5.30 \times 0.05$ mm^3) at 23 °C and 50 % relative humidity. Wet strength characterisation was performed using specimens immersed in distilled water for 24 h, with the dimensions being measured from dry specimens. Results presented are the average of five measurements.

Dynamic mechanical analysis (DMA)

Dynamic mechanical analysis was performed using A TA Instruments Q800 Dynamic Mechanical Analyser operating in tensile mode with preload force of 0.01 N, amplitude of 15 μm and frequency of 1 Hz. The storage modulus (E'), loss modulus (E''), loss tangent (tan δ) and associated glass transition (T_g) temperatures of the films were measured as a function of temperature from −30 to 150 °C at a heating rate of 3 °C·min^{-1}. Samples exhibited average dimensions of $10.00 \times 0.30 \times 0.05$ mm^3.

Material nomenclature

The nomenclature of the nanocomposites is as follows: NFC-PAA #-x, where # is the concentration of PAA by percentage weight. Crosslinked

nanocomposites are denoted by an 'x' following the PAA concentration value.

Results and discussion

Solid-state ^{13}C NMR

Figure 1 displays the solid-state ^{13}C NMR spectra of PAA and selected crosslinked and non-crosslinked NFC-PAA nanocomposites. PAA displays two peaks at 32.6 and 42.6 ppm, attributed to the CH and CH_2 groups, respectively (Vasilescu and Ponta 1996). The carboxyl carbon is assigned to the strong peak at 184.7 ppm (Maeda et al. 2011). NFC-PAA nanocomposites exhibited characteristic signals corresponding to PAA and NFC. NFC exhibited typical cellulose carbon peaks at 67.1 (C6), 77.3 (C2, C3 and C5), 85.8 (C4 amorphous domains), 91.3 (C4 crystalline domains) and 107.8 ppm (C1) (Eyholzer et al. 2010; Gilardi et al. 1995; Kono et al. 2002). As the PAA concentration increased, the CH and CH_2 peaks at 32.6 and 42.6 ppm, respectively, became more intense. Examination of the PAA carboxyl peaks at 181.5 ppm showed subtle differences between non-crosslinked and crosslinked nanocomposites. Both NFC-PAA 10-x and NFC-PAA 50-x displayed a shoulder at 186.3 ppm, while non-crosslinked nanocomposites NFC-PAA 10 and NFC-PAA 25 did not exhibit such a shoulder. The shoulder formed at 186.3 ppm is attributed to the ester COO groups formed during thermal crosslinking; however the presence of a peak at 181.5 ppm within the crosslinked nanocomposites indicates that non-reacted PAA is also present within the films.

Attenuated total reflectance infrared spectroscopy

ATR-FTIR was utilised to characterise the structure of the nanocomposites and determine the presence of crosslinking. The spectra of the nanocomposite films are presented in Fig. 2. The nanocomposites exhibited peaks characteristic of NFC and PAA structure; $\sim 3348\ cm^{-1}$ (hydrogen-bonded OH stretching of NFC), $\sim 2890\ cm^{-1}$ (-OH stretching of PAA), $\sim 1025\ cm^{-1}$ (C–O stretching within NFC) and $\sim 1705\ cm^{-1}$ (C = O stretching in PAA) (Clemons et al. 2013; Oh et al. 2005). In non-crosslinked and crosslinked films, the peak attributed to C = O stretching within PAA became sharper and more intense as PAA concentration increased.

Several differences were observed when comparing the spectra of non-crosslinked and crosslinked NFC-PAA nanocomposites. Non-crosslinked films displayed intense peaks in the region $\sim 3348\ cm^{-1}$, which are associated with hydroxyl groups bound with free water (Kondo and Sawatari 1996; Kondo 1997). In contrast, the OH bands exhibited by crosslinked nanocomposites were flatter and less intense. This indicates a reduced amount of free water within the crosslinked samples, and can be attributed to the ester

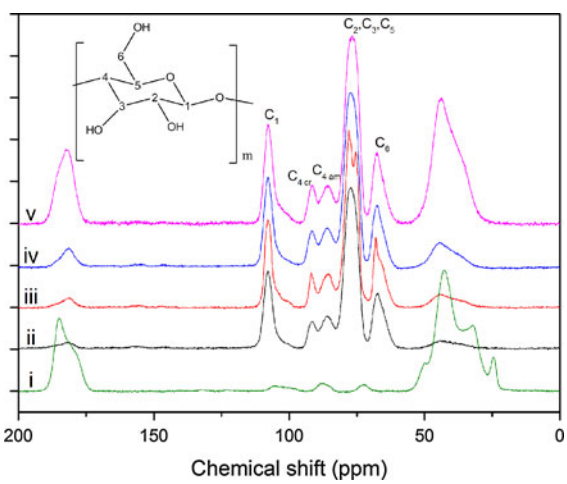

Fig. 1 ^{13}C NMR spectra; (*i*) pure PAA, (*ii*) NFC-PAA 10, (*iii*) NFC-PAA 10-x, (*iv*) NFC-PAA 25, (*v*) NFC-PAA 50-x

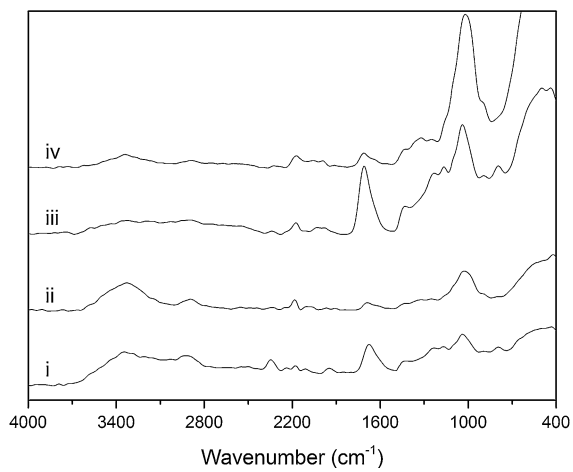

Fig. 2 ATR-FTIR spectra of NFC-PAA nanocomposites; (*i*) NFC-PAA 50, (*ii*) NFC-PAA 10, (*iii*) NFC-PAA 50-x, (*iv*) NFC-PAA 10-x

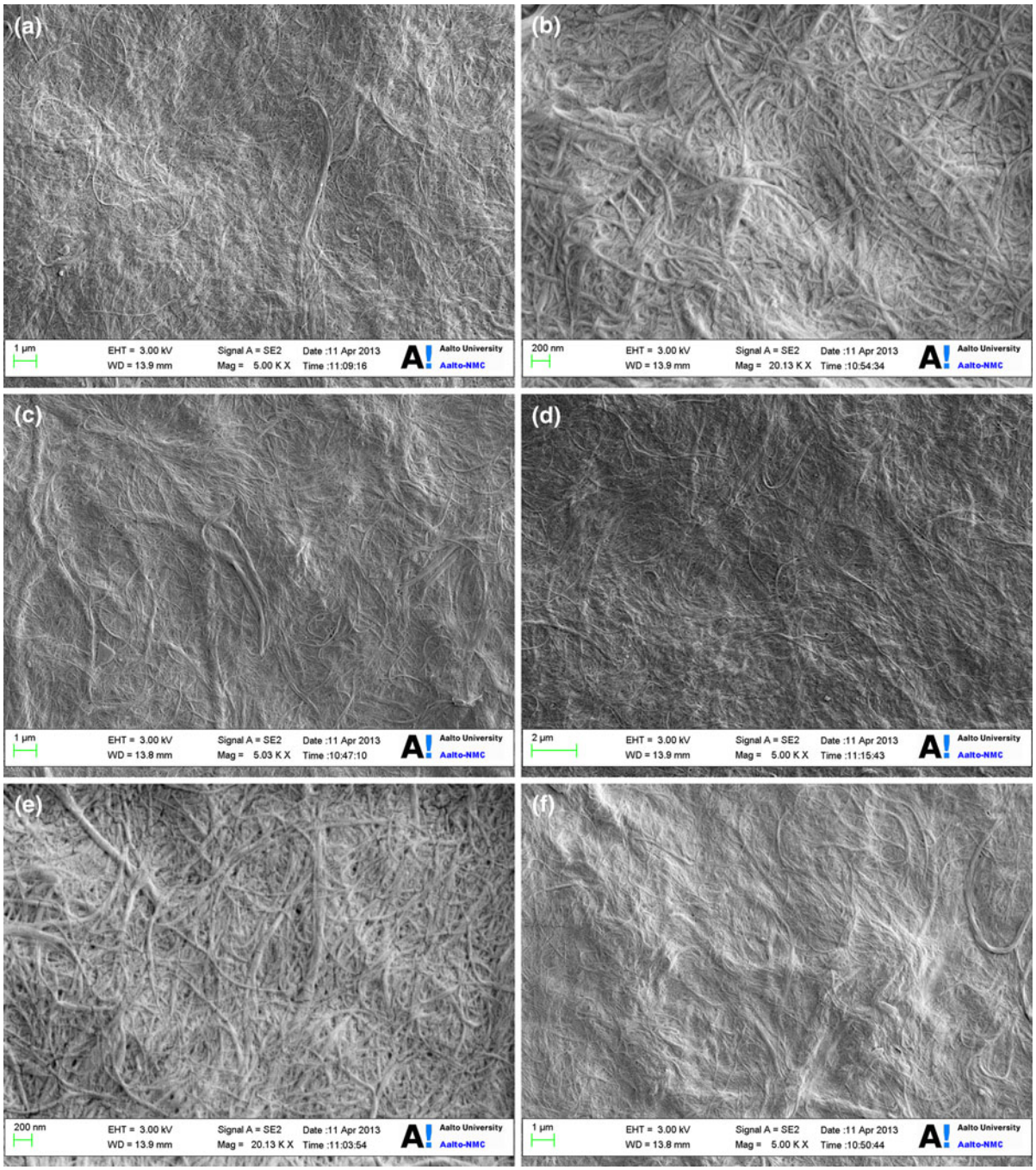

Fig. 3 Scanning electron micrographs of NFC-PAA nanocomposites; **a** NFC-PAA 5, **b** NFC-PAA 25, **c** NFC-PAA 50, **d** NFC-PAA 5-x, **e** NFC-PAA 25-x, **f** NFC-PAA 50-x

formation reaction between carboxyl groups (on PAA) and hydroxyl groups (on NFC) (Luo et al. 2013). The reduced number of unoccupied hydroxyl groups decreases the likelihood of hydrogen bonding with water molecules. In addition, the peak observed at $\sim$2,900 cm^{-1} in non-crosslinked peaks (OH stretching in PAA) reduced in intensity for crosslinked films. The carbonyl peak located at $\sim$1,705 cm^{-1} shifted

Table 1 Degree of crosslinking, water content, absorption and swelling data of NFC-PAA nanocomposites

Material	Crosslinking density (mol·cm^3)	Water content (%)	Absorbed water after 72 h (%)	Degree of swelling (%)
NFC-PAA 5	–	10.9	31.7	434.9
NFC-PAA 10	–	11.6	34.9	369.2
NFC-PAA 25	–	13.9	35.5	344.6
NFC-PAA 50	–	14.3	46.5	245.4
NFC-PAA 5-x	0.000443	6.8	18.7	215.5
NFC-PAA 10-x	0.000567	7.8	19.0	186.3
NFC-PAA 25-x	0.000591	9.3	21.3	181.7
NFC-PAA 50-x	0.001290	9.0	22.5	115.0

towards higher wavenumbers for crosslinked nanocomposites. Similar behaviour was observed by Paralikar et al. (2008) within crosslinked poly(vinyl alcohol)-cellulose nanocrystal membranes, with the shift in peak location attributed to the formation of carboxylic esters. Furthermore, the C = O peak was more intense for crosslinked films than their non-crosslinked counterparts with identical PAA concentrations. This behaviour strongly suggests that crosslinking has occurred within thermally-treated NFC-PAA films.

Scanning electron microscopy (SEM)

Scanning electron micrographs of the NFC-PAA nanocomposites are presented in Fig. 3. All films exhibited a similar surface morphology. A randomly-orientated entangled network of cellulose nanofibrils, with diameters of 30–150 nm, was evident. Some bundling or aggregation amongst NFC fibrils occurred due to strong interactions (hydrogen bonding and van der Waal's forces) between fibres. The addition of PAA caused no observable change in nanocomposite morphology, with all films displaying similar network-like structures. Although NMR and FTIR analysis confirmed interaction and bonding between the cellulose and PAA, these interactions occur without altering the surface morphology, fibre orientation or cellulose structure. No visible difference between crosslinked and non-crosslinked films was noticeable.

Crosslinking density, water absorption and swelling properties

The crosslinking densities, water-absorbed percentages and degree of swelling of the nanocomposite films are presented in Table 1. NFC-PAA 5-x displayed a crosslinking density of 0.000443 mol cm^3. Increasing the PAA concentration raised the crosslinking density to 0.000567 (NFC-PAA 10-x) and 0.000591 mol cm^3 (NFC-PAA 25-x) before reaching a maximum of 0.00129 mol cm^3 (NFC-PAA 50-x). At high loadings of PAA, the NFC hydroxyl groups are in greater proximity to the carboxyl groups of PAA, allowing for an increased likelihood of bonding. Furthermore, the chance of crosslink formation is higher due to the larger volume of PAA present throughout the nanocomposite.

The mass of NFC-PAA 5 increased by 31.7 % following immersion in water. Increasing the PAA concentration to 10 wt% raised this value to 34.9 %. The mass gain continued to increase with PAA content, with NFC-PAA 50 exhibiting a maximum of 46.5 %. The water absorption abilities of PAA are well-known (Pourjavadi et al. 2008). The polar COOH groups readily interact with water molecules, leading to hydration and hydrogen bond formation. Furthermore, repulsions between negative COO- ions formed during hydration expand the polymer chains. The likelihood of this behaviour increases with PAA concentration. Crosslinked NFC-PAA films also exhibited an increase in water absorption with PAA concentration, ranging from 18.7 % (NFC-PAA 5-x) to 22.5 % (NFC-PAA 50-x). However, crosslinked nanocomposites exhibited significantly less water-uptake than equivalent non-crosslinked materials. Introducing crosslinking into the films creates ester linkages between NFC and PAA, reducing chain mobility and reducing the total number of hydroxyl and carboxyl groups within the nanocomposites (Paralikar et al. 2008). This leads to reduced hydrophilicity and water absorption potential.

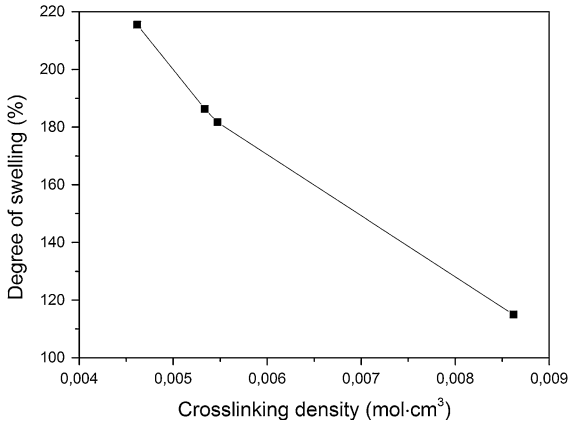

Fig. 4 Degree of swelling as a function of crosslink density of crosslinked NFC-PAA films

Although water retention increased with PAA concentration, the degree of swelling displayed an inverse relationship to PAA content. This suggests that although PAA is susceptible to water absorption, the stability of the nanocomposite as a whole (in relation to swelling) is maintained. Introduction of PAA reduces the total free volume available for swelling and solvent penetration within the nanocomposites. The degree of swelling was further diminished by the introduction of crosslinking, decreasing linearly as the crosslink density increased up to and including 25 wt% PAA concentration before deviating at 50 wt% (Figure 4). Swantomo and Megasari (2013) observed similar behaviour in crosslinked cellulose hydrogels. The introduction of crosslinks into the NFC network imparts further restrictions on chain segments, leading to a greater reduction in free volume and more compact structure.

Thermal stability and degradation

Figure 5a displays the mass loss curves of non-crosslinked NFC-PAA nanocomposites, while crosslinked nanocomposite mass loss curves are presented in Figure 5b. All materials displayed degradation curves with similar characteristics; a slight decrease in mass is observed beginning at ~67 °C and is attributed to the release of residual water within the films. This is followed by a second degradation step commencing at ~200 °C during which anhydride-type structures are formed and subsequently decarboxylated (Dubinsky et al. 2004). The large, third mass step (starting temperature ~250 °C) involves thermal cracking of NFC (Liu et al. 2011). A final mass loss event begins at ~355 °C during which chain scission and depolymerisation of PAA occur, leading to the formation of short chain fragments (McNeill and Sadeghi 1990). As the PAA fraction within the nanocomposites was increased, the percentage mass during the decarboxylation (for PAA) and thermal cracking (for NFC) stages changed correspondingly. This was due to the amount of NFC or PAA available to undergo degradation decreasing or increasing, respectively. Furthermore, increasing the PAA concentration shifted the curves towards higher temperatures, indicating an increase in degradation temperature.

The deterioration in thermal stability observed in the non-crosslinked nanocomposite can be attributed to the nature of interactions between NFC and PAA (that is, hydrogen bonding). The presence of weakly-bound or free PAA (or other acids) within the NFC nanocomposites can catalyse hydrolysis during thermal degradation (Area and Cheradame 2011), accelerating the breakdown of NFC. Likewise, the presence of moisture can encourage hydrolysis and subsequent degradation within cellulosic materials (Kučerová et al. 2007). This is correlates to the water absorption data, which showed an increase in water content with increasing PAA concentration.

The derivative mass loss curves of the nanocomposites are displayed in Figure 5c. The temperature at which the maximum rate of degradation occurs (T_d) was determined from the peak of the degradation events. NFC-PAA 5 exhibited T_d values of 326 °C (NFC thermal cracking, Td-NFC) and 378 °C (PAA chain scission and depolymerisation, T_d-PAA). The addition of 10 wt% PAA reduced T_d-NFC to 324 °C and increased T_d-PAA to 381 °C. Td-NFC diminished further with the incorporation of 25 wt% PAA, before returning to 326 °C at a PAA loading of 50 wt%. T_d-PAA continued to increase with PAA concentration, with NFC-PAA 50 displaying a T_d-PAA of 395 °C. In contrast, crosslinked nanocomposites displayed an increase in both T_d-NFC and T_d-PAA with PAA loading. NFC-PAA 5-x exhibited T_d-NFC and T_d-PAA values of 327 and 398 °C. Peak degradation temperatures continued to increase for NFC-PAA10-x (T_d-NFC = 328 °C, T_d-PAA = 381 °C), NFC-PAA 25-x (T_d-NFC = 331 °C, T_d-PAA = 384 °C) and NFC-PAA 50-x (T_d-NFC = 333 °C, T_d-

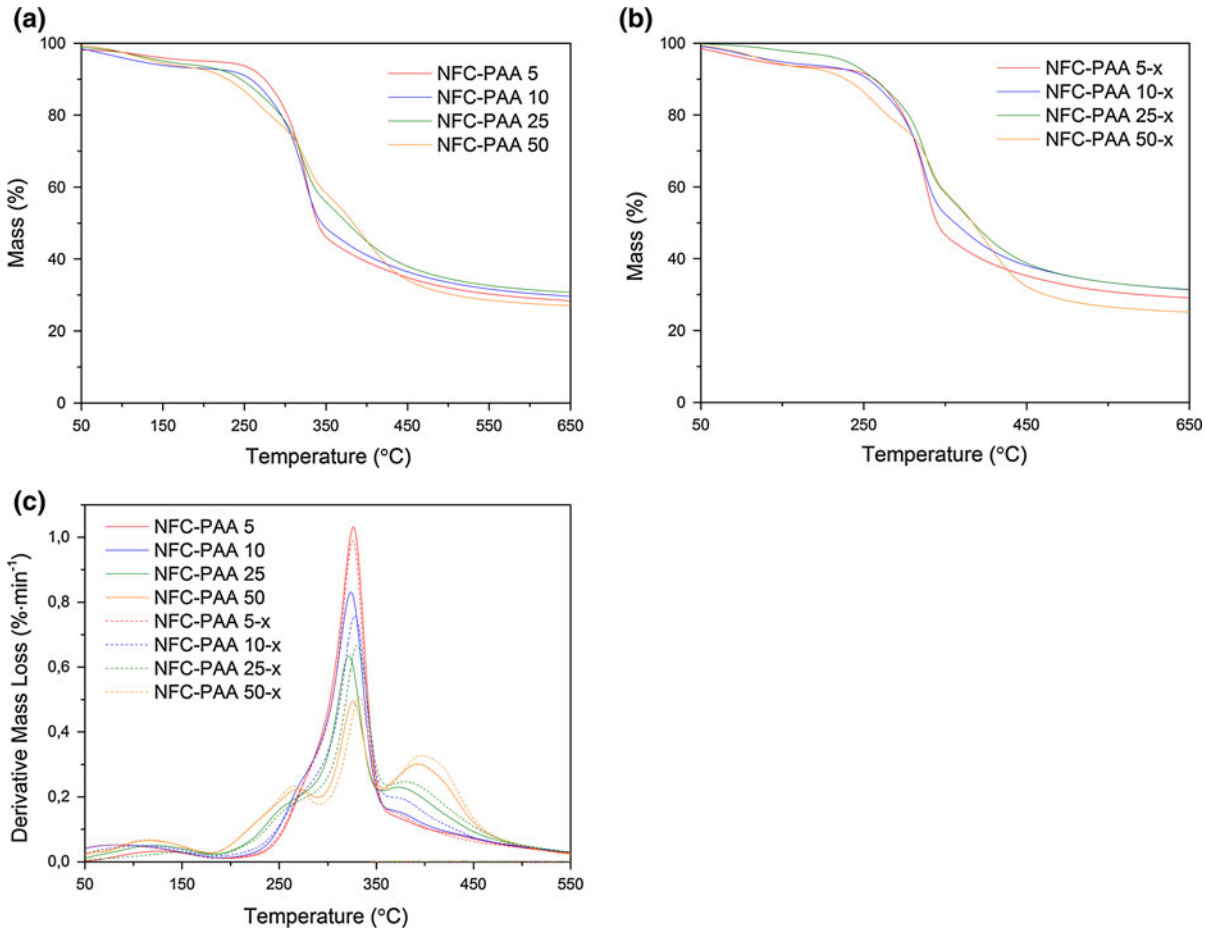

Fig. 5 Thermal degradation behaviour of NFC-PAA nanocomposites; **a** mass loss curves of non-crosslinked NFC-PAA films, **b** mass loss curves of crosslinked NFC-PAA films, **c** derivative mass loss curves of NFC-PAA films

PAA = 398 °C). Furthermore, crosslinked NFC-PAA nanocomposites displayed higher T_d-NFC and T_d-PAA values than their non-crosslinked counterparts for identical PAA concentrations.

In the case of the crosslinked NFC-PAA nanocomposites, stronger ester linkages are formed between hydroxyl groups and carboxylic acid. Although some unbound PAA may remain within the nanocomposites, the amount is significantly less when compared to non-crosslinked NFC-PAA. In addition, water absorption analysis confirmed a reduced amount of moisture within the crosslinked nanocomposites, since ester bonds occupy NFC hydroxyl groups. This leads to a reduction in hydrolysis rate during thermal degradation. Furthermore, the introduction of crosslinks into the composites increased thermal stability by restricting molecular rotations and vibrations that occur within polymers when thermally excited (Dutta 2012). As a polymer is heated and begins to degrade, macromolecule chains must break-up or de-bond into smaller segments that can be eliminated from the bulk structure. Crosslinking causes the formation of larger-than-usual fragments, which require more energy to break into portions small-enough to be eliminated.

Thermomechanical analysis

Stress–strain analysis

The stress–strain curves of the nanocomposites are displayed in Figure 6a, while the mechanical data is summarised in Table 2. NFC-PAA 5 displayed a Young's modulus of 17.7 GPa and breaking stress of 311.3 MPa. Increasing the PAA concentration to

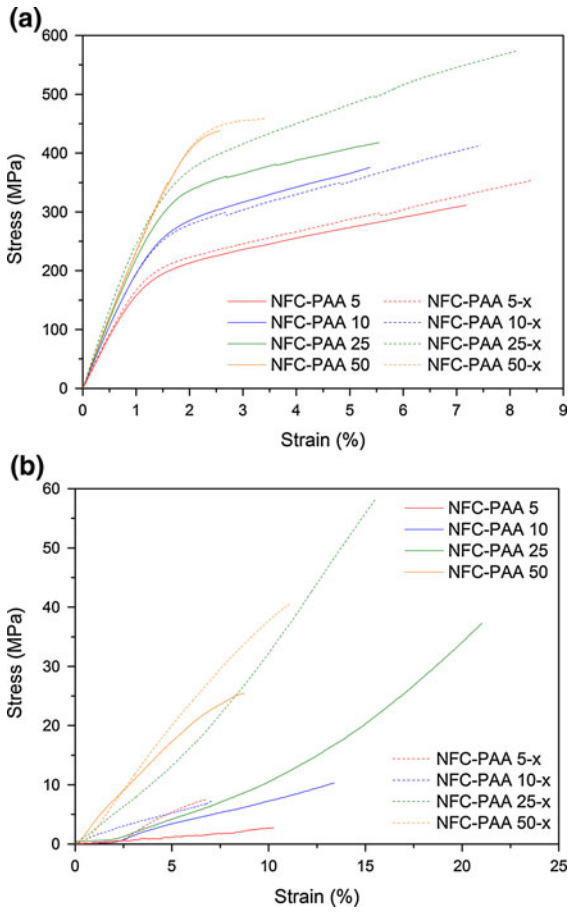

Fig. 6 Stress-strain curves of NFC-PAA nanocomposites; **a** tested at 23 °C and 50 % relative humidity, **b** tested following immersion in water for 24 h

10 wt% raised the modulus to 21.1 GPa while the stress at break increased to 375.4 MPa. For the non-crosslinked nanocomposites, Young's modulus and stress at break reached maximum values of 24.2 GPa and 437.6 MPa, respectively with NFC-PAA 50. The strain at break diminished with PAA concentration, ranging from 7.2 (NFC-PAA 5) to 2.6 % (NFC-PAA 10). Crosslinked films experienced an increase in Young's modulus with the addition of PAA, increasing from 18.5 (NFC-PAA 5-x) to 26.6 GPa (NFC-PAA 25-x). Similarly, the stress at break increased from 353.1 to 562.2 MPa with respective PAA concentrations of 5 and 25 wt%. NFC-PAA 50-x exhibited lower modulus and breaking stress values than NFC-PAA 25-x, however the values were still larger than its non-crosslinked equivalent, NFC-PAA 50. The strain at break of the crosslinked composites gradually diminished with increasing PAA content.

A clear dependence of tensile mechanical behaviour on NFC/PAA concentration and the nature of inter-component interactions are evident. Luo et al. (2013) described how regenerated cellulose and PAA can form a semi-interpenetrating network. The strong interfacial interaction (hydrogen bonding) between the NFC and PAA determines the mechanical properties of the films. These interactions, in the form of hydrogen bonds, impart restrictions on segments of polymer chain leading to enhanced stiffness and strength. One consequence of the restricted ability of polymer chains to rotate about bonds and slide past one another is the observed reduction in ductility.

In addition to component concentration, crosslinking exhibited a profound effect on tensile properties. At identical PAA concentrations, crosslinked NFC-PAA films displayed superior Young's modulus and strength values when compared to their non-crosslinked counterparts. Lu and Hsieh (2009) observed similar behaviour in cellulose nanocrystal-reinforced PAA fibres. The covalent bonds formed during the esterification reaction are stronger and more robust than the hydrogen bonding that occur between non-crosslinked NFC and PAA. These covalent bonds (in conjunction with hydrogen bonds) allow for greater restrictions to be placed on segmental chain motions, enhancing material strength and facilitating greater stress-bearing capacity. Furthermore, as the PAA concentration is increased the crosslinking density is also likely to rise. This allows for more restrictions and reinforcement ability to be imparted on the NFC.

The introduction of crosslinks proved an efficient method of retaining elongation at break, while enhancing mechanical strength and toughness. Salmah et al. (2008) observed similar retainment of elasticity in vulcanised paper sludge-polypropylene-EPDM rubber composites. The enhanced elastic properties were attributed to superior interfacial interaction between the composite components, facilitated by the introduction of crosslinks. The reduced Young's modulus and breaking stress values displayed by NFC-PAA 50-x may be explained in terms of composite structure. Within the 50 wt% filled crosslinked film, the structure is highly constrained due to the presence of ester bonds and highly packed due to the large PAA content. This may limit the total number of PAA carboxyl groups able to interact with NFC hydroxyl groups. As a consequence, unbound PAA may retain water and reduce mechanical properties. Water

Table 2 Stress-strain data of NFC-PAA nanocomposites

Material number	Tested at 23 °C and 50 % relative humidity			Films immersed in water for 24 h		
	Tensile modulus (GPa)	Break stress (MPa)	Elongation at break (%)	Tensile modulus (MPa)	Break stress (MPa)	Elongation at break (%)
NFC-PAA 5	17.7 ± 2.5	311.3 ± 10.8	7.2 ± 0.4	240 ± 0.9	2.8 ± 5.8	10.2 ± 0.4
NFC-PAA 10	21.1 ± 1.8	345.4 ± 7.1	5.4 ± 0.3	302 ± 3.1	10.2 ± 8.3	13.3 ± 1.8
NFC-PAA 25	23.3 ± 3.4	417.9 ± 5.4	5.6 ± 0.3	509 ± 2.4	37.4 ± 8.4	21.0 ± 3.8
NFC-PAA 50	24.2 ± 5.7	437.6 ± 10.2	2.6 ± 1.9	3621 ± 5.8	25.4 ± 7.5	8.7 ± 1.2
NFC-PAA 5-x	18.5 ± 2.9	355.1 ± 6.1	8.4 ± 0.4	786 ± 2.8	7.4 ± 2.5	6.8 ± 1.0
NFC-PAA 10-x	23.1 ± 4.7	413.1 ± 9.5	7.5 ± 1.5	1222 ± 3.0	7.5 ± 3.9	7.1 ± 0.6
NFC-PAA 25-x	26.6 ± 4.2	562.2 ± 8.2	8.2 ± 0.2	2544 ± 6.9	58.4 ± 7.1	15.5 ± 1.4
NFC-PAA 50-x	25.3 ± 3.8	458.8 ± 4.6	3.4 ± 1.3	3570 ± 9.4	40.5 ± 9.7	11.2 ± 2.7

molecules can compete with PAA to hydrogen bond with NFC, changing the behaviour of the amorphous regions of cellulose and diminishing mechanical properties (Myllytie et al. 2010; Zhou et al. 2001). However, NFC-PAA 50-x exhibited superior tensile properties than NFC-PAA 50, suggesting that despite the high PAA loading, sufficient interfacial adhesion and interaction was achieved to enhance film properties.

The wet-strength tensile properties of the nanocomposites (Figure 6b), displayed similar trends to films tested under dry conditions. Young's modulus and tensile strength increased with PAA concentration, as the degree of restrictions imparted on chain motion increased. Crosslinked samples displayed higher modulus and breaking stress values due to greater reinforcement and hindrance on chain motion provided by ester bonds between the NFC and PAA. The use of crosslinks to enhance both dry- and wet-strength properties of cellulosic materials is well documented (Gärdlund et al. 2003; Hubbe 2006; Pahimanolis et al. 2013). Elasticity increased with PAA concentration, which can be attributed to two factors. Firstly, cellulose is readily plasticised by water due to its polar structure. Water molecules disrupt existing hydrogen bonds between cellulose fibres, increasing the free volume and reducing hindrance to local chain mobility (Jafarpour et al. 2007). Secondly, PAA's ability to retain water encourages a greater degree of plasticisation. Water absorption analysis determined that water retention increased with PAA concentration and that crosslinking retards water uptake by increasing film hydrophobicity. The wet-strength data correlates accordingly, where the more-hydrophobic crosslinked films displayed lower elongation at break values than non-crosslinked nanocomposites. The results highlight the effectiveness of crosslinking to enhance the tensile properties and mechanical stability of materials subjected to aqueous environments.

Dynamic mechanical analysis

The storage moduli (E') of the NFC-PAA nanocomposites are presented in Figure 7a while the E' and T_g values are summarised in Table 3. NFC-PAA 5 displayed a E' value of ~17.2 GPa at −30 °C. Increasing the PAA content caused a corresponding increase in E', ranging from 19.1 (NFC-PAA 10) to 22.5 GPa (NFC-PAA 25). This behaviour is indicative of the PAA chains' ability to restrict segmental motion and impart stiffness into the nanocomposites. Crosslinked films displayed higher E' values of 19.6 (NFC-PAA 5-x), 19.9 (NFC-PAA 10-x) and 21.2 GPa (NFC-PAA 25-x) compared with non-crosslinked NFC-PAA films, attributed to stronger interfacial adhesion via esterification. Nanocomposites containing up-to and including 25 wt% PAA continued to maintain larger E' values than NFC-PAA 5, confirming that reinforcement occurs at temperatures above T_g. Both NFC-PAA 50 and NFC-PAA 50-x displayed a reduction in E' at −30 °C relative to films filled with 25 wt% PAA, as well as displaying lower E' values than NFC-PAA 5 at temperatures above T_g.

The loss moduli (E'') of the nanocomposites are presented in Figure 7b. The T_g was obtained from the E'' curves' peak since that is where maximum heat dissipation occurs. NFC-PAA 5 exhibited a T_g of

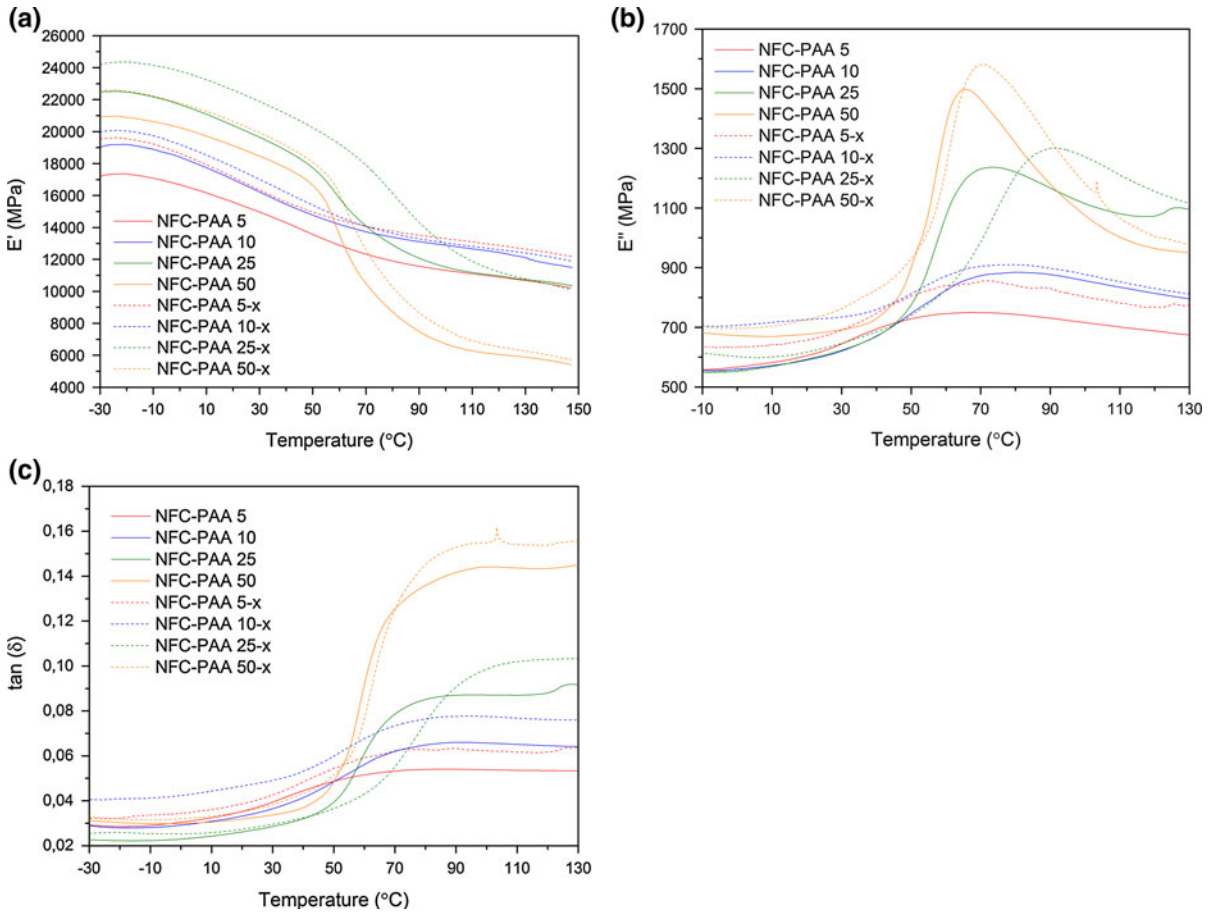

Fig. 7 Dynamic mechanical properties of NFC-PAA nanocomposites; **a** storage modulus, **b** loss modulus, **c** loss tangent (tan δ)

67.2 °C, which increased to 79.7 °C with the addition of 10 wt% PAA. Further PAA loading caused the T_g to drop to 73.2 (NFC-PAA 25) and 65.4 °C (NFC-PAA 50). Crosslinked films experienced increased T_g with PAA content, reaching a maximum of 90.1 °C at a concentration of 25 wt%. However, as the PAA content becomes greater, the T_g shifts towards lower temperatures. Chung et al. (2004) observed a similar drop in T_g with increasing crosslink density for starch. The reduction was attributed to the high water- affinity and retention capacity of the phosphate-based cross-linking agents, leading to internal plasticisation. Similar reasoning can be applied to NFC-PAA films, being further supported by the water absorption and wet-strength data.

Despite the reduction in T_g, the increased E' values with PAA content indicate sufficient interaction between the PAA and NFC occurs within the nano-composites. The dynamic mechanical data suggests that within the NFC-PAA films, two competing mechanisms are present; (a) the ability of PAA to interact, reinforce and restrict NFC chain motion, and (b) the ability of PAA (and NFC) to interact with and adsorb water molecules.

The loss tangent (tan δ) of the films are displayed in Figure 7c. Although the tan δ plateaued above the T_g rather than producing a distinctive peak, the shift in T_g and curve location with PAA loading was similar in behaviour to the E" curves. Peak amplitude increased with PAA concentration. Peak amplitude provides an indication of the number of kinetic units mobile enough to contribute to the glass–rubber transition (Kennedy et al. 2009). Damping ability within polymer composites is believed to be influenced by two factors: (a) the amount of free volume, (b) internal friction between the filler and matrix and between the filler particles themselves across the glass transition region (Trakulsujaritchok and Hourston 2006). The

Table 3 Dynamic mechanical data of NFC-PAA nanocomposites

Material	E' at −30 °C (GPa)	E' at 130 °C (GPa)	T_g from E" peak max. (°C)
NFC-PAA 5	17.3	10.8	67.2
NFC-PAA 10	19.1	12.1	79.7
NFC-PAA 25	21.0	10.7	73.2
NFC-PAA 50	22.6	5.8	65.4
NFC-PAA 5-x	19.5	12.6	70.3
NFC-PAA 10-x	20.0	12.3	80.0
NFC-PAA 25-x	28.6	10.7	91.3
NFC-PAA 50-x	22.6	6.4	70.3

latter increases as the number of chain movements become greater, leading to an increase in damping ability. Increasing the PAA concentration also increases the amount of water within the nanocomposites, allowing films to experience greater chain motion due to increased free volume and plasticisation. This results in greater internal friction within the films and subsequently enhances damping properties.

Conclusion

Solvent casting was utilised to prepare nanocomposites of nanofibrillated cellulose (NFC) and poly(-acrylic acid) (PAA). Thermally-induced crosslinking led to the formation of ester bonds, as confirmed by ^{13}C NMR and FTIR. A randomly-orientated network structure was evident in all films, with PAA and crosslinking displaying no visible effect on film morphology. Water absorption increased with PAA concentration, while the degree of swelling for the entire nanocomposite decreased. Crosslinking proved an effective method of restricting water uptake and swelling, by reducing the total number of hydroxyl and carboxyl groups able to interact with water molecules and prevent repulsion amongst ions. Thermal stability was enhanced by the introduction of crosslinks due to restrictions imparted on chain motions, increasing the activation energy for degradation.

Young's modulus and break strength increased with PAA concentration, facilitated by effective interaction between the PAA and NFC. Tensile properties were further enhanced by crosslinking and ductility was maintained, due to restraints imparted on segments of polymer chain. Wet-strength tensile properties were similarly enhanced by crosslinking, due to the increased hydrophobicity of the nanocomposites. Non-crosslinked films displayed better elasticity following immersion in water, attributed to the plasticising effect of water. The glass transition temperature increased up to 10 and 25 wt% PAA concentration in non-crosslinked and crosslinked films, respectively. Higher PAA loading caused a decrease due to increased water content, resulting in internal plasticisation. Crosslinking proved to be a suitable method of enhancing the thermomechanical, thermal and water absorption properties of NFC, particularly in aqueous environments.

References

Al-Turaif HA (2013) Relationship between tensile properties and film formation kinetics of epoxy resin reinforced with nanofibrillated cellulose. Prog Org Coat 76:477

Area MC, Cheradame H (2011) Paper aging and degradation: recent findings and research methods. Bioresources 6:5307–5337

Baştürk E, Demir S, Daniş Ö, Kahraman MV (2013) Covalent immobilization of α-amylase onto thermally crosslinked electrospun PVA/PAA nanofibrous hybrid membranes. J Appl Polym Sci 127:349–355

Cho M, Park B (2011) Tensile and thermal properties of nanocellulose-reinforced poly(vinyl alcohol) nanocomposites. J Indust Eng Chem 17:36–40

Chung H, Woo K, Lim S (2004) Glass transition and enthalpy relaxation of cross-linked corn starches. Carbohydr Polym 55:9–15

Clemons C, Sedlmair J, Illman B, Ibach R, Hirschmugl C (2013) Chemically imaging the effects of the addition of nanofibrillated cellulose on the distribution of poly(acrylic acid) in poly(vinyl alcohol). Polymer 54:2058–2061

Dubinsky S, Grader GS, Shter GE, Silverstein MS (2004) Thermal degradation of poly(acrylic acid) containing copper nitrate. Polym Degrad Stab 86:171–178

Dubolazov A, Nurkeeva Z, Mun G, Khutoryanskiy V (2006) Design of mucoadhesive polymeric films based on blends of poly(acrylic acid) and (hydroxypropyl) cellulose. Biomacromolecules 7:1637–1643

Dutta J (2012) Synthesis and characterization of γ-irradiated PVA/PEG/CaCl2 hydrogel for wound dressing. Amer J Chem 2:6–11

Endo R, Saito T, Isogai A (2013) TEMPO-oxidized cellulose nanofibril/poly(vinyl alcohol) composite drawn fibers. Polymer 54:935

Eyholzer C, Bordenau N, Lopez-Suevos F, Rentsch D, Zimmermann T, Oksman K (2010) Preparation and characterization of water-redispersible nanofibrillated cellulose in powder form. Cellulose 17:19–30

Fox DM, Lee J, Zammarano M, Katsoulis D, Eldred DV, Haverhals LM, Trulove PC, De Long HC, Gilman JW (2012) Char-forming behavior of nanofibrillated cellulose treated with glycidyl phenyl POSS. Carbohydr Polym 88:847–858

Fujisawa S, Ikeuchi T, Takeuchi M, Saito T, Isogai A (2012) Superior reinforcement effect of TEMPO-oxidized cellulose nanofibrils in polystyrene matrix: optical, thermal, and mechanical studies. Biomacromolecules 13:2188–2194

Gärdlund L, Wågberg L, Gernandt R (2003) Polyelectrolyte complexes for surface modification of wood fibres: II. Influence of complexes on wet and dry strength of paper. Colloids Surf Physicochem Eng Aspects 218:137–149

Gilardi G, Abis L, Cass AEG (1995) Carbon-13 CP/MAS solid-state NMR and FT-IR spectroscopy of wood cell wall biodegradation. Enzyme Microb Technol 17:268–275

Hubbe M (2006) Bonding between cellulosic fibers in the absence and presence of dry-strength agents—a review. Bioresources 1:281–318

Jafarpour G, Roig F, Dantras E, Boudet AM, Lacabanne C (2007) Influence of water on localized and delocalized molecular mobility of cellulose. J Non-Cryst Sol 3:4108–4115

Kennedy JE, Lyons JG, Geever LM, Higginbotham CL (2009) Synthesis and characterisation of styrene butadiene styrene-g-acrylic acid for potential use in biomedical applications. Mater Sci Eng, C 29:1655–1661

Kim DS, Park HB, Rhim JW, Lee YM (2005) Proton conductivity and methanol transport behavior of cross-linked PVA/PAA/silica hybrid membranes. Solid State Ionics 176:117–126

Klemm D, Kramer F, Moritz S, Lindström T, Ankerfors M, Gray D, Dorris A (2011) Nanocelluloses: a new family of nature-based materials. Angew Chem Inter Ed 50:5438–5466

Kondo T (1997) The assignment of IR absorption bands due to free hydroxyl groups in cellulose. Cellulose 4:281–292

Kondo T, Sawatari C (1996) A Fourier transform infra-red spectroscopic analysis of the character of hydrogen bonds in amorphous cellulose. Polymer 37:393–399

Kono H, Yunoki S, Shikano T, Fujiwara F, Erata T, Takai M (2002) CP/MAS 13C NMR study of cellulose and cellulose derivatives. 1. Complete assignment of the CP/MAS ^{13}C NMR spectrum of the native cellulose. J Am Chem Soc 124:7506–7511

Kučerová I, Ohlídalová M, Novotná M, Michalcová A (2007) Examination of corroded wood by ammonium phosphate and sulphate-based fire retardants—the results of the prague castle roof timber examination ICOMOS IWC - XVI International Symposium, Florence, Venice and Vicenza, 11th–16th Nov 2007, pp 1–4

Kumeta K, Nagashima I, Matsui S, Mizoguchi K (2003) Crosslinking reaction of poly(vinyl alcohol) with poly(-acrylic acid) (PAA) by heat treatment: effect of neutralization of PAA. J Appl Polym Sci 90:2420–2427

Lee S, Mohan DJ, Kang I, Doh G, Lee S, Han S (2009) Nanocellulose reinforced PVA composite films: effects of acid treatment and filler loading. Fiber Polym 10:77–82

Li L, Hsieh Y (2005) Ultra-fine polyelectrolyte hydrogel fibres from poly(acrylic acid)/poly(vinyl alcohol). Nanotechnology 16:2852

Littunen K, Hippi U, Saarinen T, Seppälä J (2013) Network formation of nanofibrillated cellulose in solution blended poly(methyl methacrylate) composites. Carbohydr Polym 91:183

Liu A, Walther A, Ikkala O, Belova L, Berglund LA (2011) Clay nanopaper with tough cellulose nanofiber matrix for fire retardancy and gas barrier functions. Biomacromolecules 12:633–641

Loría-Bastarrachea MI, Carrillo-Escalante HJ, Aguilar-Vega MJ (2002) Grafting of poly(acrylic acid) onto cellulosic microfibers and continuous cellulose filaments and characterization. J Appl Polym Sci 83:386–393

Lu P, Hsieh L (2009) Cellulose nanocrystal-filled poly(acrylic acid) nanocomposite fibrous membranes. Nanotechnology 20:415604

Luo H, Hu J, Zhu Y, Wu J, Zhang S, Fan Y, Ye G (2013) Mechanically adaptive cellulose-poly(acrylic acid) polymeric composites in wet/dry cycles. J Appl Polym Sci 127:675–681

Maeda S, Fujiwara Y, Sasaki C, Kunimoto Ko-Ki (2011) Structural analysis of microbial poly(ε-$_{L}$-lysine)/poly(-acrylic acid) complex by FT-IR, DSC, and solid-state ^{13}C and ^{15}N NMR. Polym J 44:200–203

McNeill IC, Sadeghi SMT (1990) Thermal stability and degradation mechanisms of poly(acrylic acid) and its salts: part 1—poly(acrylic acid). Polym Degrad Stab 29:233–246

Moon RJ, Martini A, Nairn J, Simonsen J, Youngblood J (2011) Cellulose nanomaterials review: structure, properties and nanocomposites. Chem Soc Rev 40:3941–3994

Myllytie P, Salmén L, Haimi E, Laine J (2010) Viscoelasticity and water plasticization of polymer-cellulose composite films and paper sheets. Cellulose 17:375–385

Nakagaito AN, Yano H (2005) Novel high-strength biocomposites based on microfibrillated cellulose having nano-order-unit web-like network structure. Appl Phys A 80:155–159

Nikolaeva O, Budtova T, Alexeev V, Frenkel S (2000) Interpolymer complexation between polyacrylic acid and cellulose ethers: formation and properties. J Polym Sci, Part B: Polym Phys 38:1323–1330

Nogi M, Handa K, Nakagaito AN, Yano H (2005) Optically transparent bionanofiber composites with low sensitivity to refractive index of the polymer matrix. Appl Phys Lett 87:243110

Oh SY, Yoo DI, Shin Y, Seo G (2005) FTIR analysis of cellulose treated with sodium hydroxide and carbon dioxide. Carbohydr Res 340:417–428

Pahimanolis N, Salminen A, Penttilä PA, Korhonen JT, Johansson L, Ruokolainen J, Serimaa R, Seppälä J (2013) Nanofibrillated cellulose/carboxymethyl cellulose composite with improved wet strength. Cellulose 20:1459–1468

Paralikar SA, Simonsen J, Lombardi J (2008) Poly(vinyl alcohol)/cellulose nanocrystal barrier membranes. J Membr Sci 320:248–258

Peresin MS, Habibi Y, Vesterinen A, Rojas OJ, Pawlak JJ, Seppälä JV (2010) Effect of moisture on electrospun nanofiber composites of poly(vinyl alcohol) and cellulose nanocrystals. Biomacromolecules 11:2471–2477

Pourjavadi A, Soleyman R, Barajee GR (2008) Novel nanoporous superabsorbent hydrogel based on poly(acrylic

acid) grafted onto salep: synthesis and swelling behavior. Starch–Stärke 60:467–475

Priest WJ (1951) Swelling of polyvinyl alcohol in water. J Polym Sci 6:699–710

Şakar-Deliormanli A (2012) Flow behavior of hydroxypropyl methyl cellulose/polyacrylic acid interpolymer complexes in aqueous media. Polym Int 61:1751–1757

Salmah H, Ismail H, Bakar AA (2008) The effects of dynamic vulcanization and compatibilizer on properties of paper sludge-filled polypropylene/ethylene propylene diene terpolymer composites. J Appl Polym Sci 107:2266–2273

Srithep Y, Turng L, Sabo R, Clemons C (2012) Nanofibrillated cellulose (NFC) reinforced polyvinyl alcohol (PVOH) nanocomposites: properties, solubility of carbon dioxide, and foaming. Cellulose 19:1209–1223

Swantomo D, Megasari K (2013) Synthesis of controlled release fertilizers based on smart biodegradable hydrogel cellulose-vinyl monomers using radiation. Indonesia Toray Science Foundation Seminar on Science and Technology Session, Vol. A, pp 1–9

Syverud K, Kirsebom H, Hajizadeh S, Chinga-Carrasco G (2011) Cross-linking cellulose nanofibrils for potential elastic cryo-structured gels. Nanoscale Res Lett 6:626

Trakulsujaritchok T, Hourston DJ (2006) Damping characteristics and mechanical properties of silica filled PUR/PEMA simultaneous interpenetrating polymer networks. Euro Polym J 42:2968–2976

Vasilescu AS, Ponta CC (1996) A ^{13}C-NMR study of polyacrylic acid gels as radioactive ion sorbents. Prog Colloid Polym Sci 102:98–100

Zhou, Tashiro K, Hongo T, Shirataki H, Yamane C, Ii T (2001) Influence of water on structure and mechanical properties of regenerated cellulose studied by an organized combination of infrared spectra, X-ray diffraction, and dynamic viscoelastic data measured as functions of temperature and humidity. Macromolecules 34:1274–1280